DOI: 10.1002/adma.202002329
Article type: Communication

Title: A 13.56 MHz Rectifier Based on Fully Inkjet Printed Organic Diodes

*Fabrizio A. Viola, Biagio Brigante, Paolo Colpani, Giorgio Dell'Erba, Virgilio Mattoli, Dario Natali and Mario Caironi**

Dr. F. A. Viola, B. Brigante, P. Colpani, Dr. G. Dell'Erba, Prof. Dario Natali, Dr. M. Caironi
Center for Nano Science and Technology @PoliMi, Istituto Italiano di Tecnologia, via Pascoli 70/3, 20133 Milano, Italy.
E-mail: mario.caironi@iit.it
Dr. V. Mattoli
Center for Micro-BioRobotics, Istituto Italiano di Tecnologia, viale Rinaldo Piaggio 34, 50125 Pontedera (PI), Italy
Prof. D. Natali
Dipartimento di Elettronica, Informazione e Bioingegneria, Politecnico di Milano, via Ponzio 34/5, 20133 Milano, Italy

Keywords: printed electronics, RFID, diode, rectifier, organic semiconductors

Abstract:

The increasing diffusion of portable and wearable technologies results in a growing interest in electronic devices having features such as flexibility, lightness-in-weight, transparency and wireless operation. Organic electronics was proposed as a potential candidate to fulfill such needs, in particular targeting pervasive Radio-Frequency (RF) applications. Still, limitations in terms of device performances at RF, particularly severe when large-area and scalable fabrication techniques are employed, have largely precluded the achievement of such an appealing scenario. In this work, the rectification of an electromagnetic wave at 13.56 MHz with a fully inkjet printed polymer diode is demonstrated. The rectifier, a key enabling component of future pervasive wireless systems, is fabricated through scalable large-area methods on plastic. To provide a proof-of-principle demonstration of its future applicability, its adoption in powering a printed integrated polymer circuit is presented. The possibility of harvesting electrical power from RF waves and delivering it to a cheap flexible substrate

through a simple printed circuitry paves the way to a plethora of appealing distributed electronic applications.

Main text:

The rising demand for automatic identification procedures has resulted in an increasing request of portable and pervasive devices, such Radio-Frequency IDentification (RFID) tags, which could be used, for example, to identify everyday objects through electronic serialization codes. In general, RFID devices can be classified depending on the frequency at which they operate. Low-frequency (LF) RFID tags work at 120-145 kHz (LF), high-frequency (HF) tags at 13.56 MHz (HF), and ultra high-frequency (UHF) tags operate at frequencies higher than 860 MHz.[1] Another typical classification of RFID devices is related to the presence or not of a power supply or battery. Active RFID tags contain their own power source giving them the ability to broadcast with a read range of up to 100 meters (far-field communication protocols), so they typically operate in the UHF regime. Passive RFIDs do not have any power supply: all the power required for operating the tag is generated by converting the alternating-current (AC) RF signal received from an antenna into a direct-current (DC) power supply. Thus, the RFID tag usually contains a low resistance antenna and a high-frequency rectifier for AC to DC conversion. Passive RFID tags usually can be read from few cm for proximity readers (near-field communication protocol) and up to 1 m for vicinity readers. Choice of the specific RFID device depends on the target application and it is typically a trade-off among required reading distance, costs and technological constraints. Cost-effective passive tags are more suited for high volume products of limited intrinsic value and the HF range is preferable where bulky coils, such as those required for LF, are not an option, and tag flexibility and ease of integration are prerequisites.[1] Therefore, passive 13.56 MHz RFIDs are an appealing option for low-cost RF tagging of mass produced products.

Towards such scenario, in the last two decades, large-area compatible semiconductor technologies have been studied with the goal of ensuring future scalable manufacturing of RFID tags at drastically reduced costs. Within such framework, solution-processable semiconductors are one of the most promising choices, as they can be deposited by high-throughput printing techniques.[2]

In recent years, the use of liquid silicon or silicon microparticles as semiconducting materials has been deeply investigated with the aim to combine the advantage of solution processing and the well-known electronic performance, stability and reproducibility of Si.[3] To date, interesting examples of solution-processable diodes based on liquid silicon or Si-microparticles have been reported in literature.[4] However, there are main drawbacks, such as high temperature steps (> 350 °C) needed during the fabrication process and the very high cost, which make these materials not yet fully compatible with flexible substrates and competitive for the easiness of integration.[5]

Nanomaterials, such as Carbon Nanotubes and Graphene, received an increasing interest in last decades due to their unique properties, such as mechanical flexibility and electrical performances (operation frequency, mobility etc.).[5] Among these materials, single-walled carbon nanotubes (SWCNTs) are probably the most promising for the development of high-speed electronics based on solution processable materials, such as HF or UHF diodes.[6] In fact, several methods have been explored in recent years for the development of SWCNTs inks, such as functionalization via polymer wrapping or density-gradient centrifugation, for large area fabrication process techniques.[5] However, the high cost required for the development of such inks still have limited the use of these materials and devices for mass production.[5]

Others interesting options are certainly metal oxide semiconductors (MOs), such as indium gallium zinc oxide (IGZO) and zinc oxide (ZnO), thanks to the very high performances.[7] Best performing MOs in general require high annealing temperatures and suffer from fragility to mechanical stress, which makes the compatibility of these materials with flexible substrates still

an open issue.[8] In addition, most MOs based diodes to date are fabricated through physical deposition techniques, such as sputtering or atomic layer deposition.[9] Only rare examples of fully solution processed MOs based diodes have been reported.[10]

As an alternative, organic semiconductors can offer advantages in terms of mechanical properties and low processing temperatures, therefore being strong candidates to deliver highly flexible and portable devices that can be also fabricated with scalable techniques.[11]-[13] However, even if recently electronic performances of organic devices such as sensors, circuits, solar cells and light-emitting diodes have steadily improved,[14]-[18] so far low charge carriers mobility of organic materials have largely precluded the achievement of suitably high operation frequencies. Such limitation is even more evident when large-area printing techniques are adopted to pattern semiconductors, owing to a poorer control over films microstructure, negatively affecting fundamental aspects such as charge transport. As a result, fully printed organic rectifying diodes, the key component of RF rectifiers, have failed to reach operational frequencies in the HF range.

For this reason, most of the reported organic rectifiers are based on diodes in which the semiconductor is typically a small molecule, e.g., such as pentacene or copper phthalocyanine, deposited by thermal evaporation. Despite the performances of small molecule based diode are impressive, with operational frequencies reaching the HF and even the UHF range,[19]-[20] the fabrication process requires a high vacuum or ultra-high vacuum step for the deposition of the organic semiconductor. Although organic diodes based on a solution processed polymer semiconductors capable of operating around or above 10 MHz have been demonstrated, both by employing spin-coating,[21] and roll-to-roll compatible techniques,**Errore. L'origine riferimento non è stata trovata.** there is no demonstration so far of fully printed organic diodes, because in order to achieve high performances, either one or both of the electrodes are thermally evaporated. In Table S1, in Supporting Information, we summarize and compare some previous works based on inorganic and organic diodes, compatible with large-area processes or flexible substrates,

highlighting the fabrication process and figures of merit. In this work, by adopting a printable polymer semiconductor with enhanced out-of-plane transport properties and by thorough device engineering, we demonstrate a 13.56 MHz rectifier based on fully inkjet printed organic diodes. We propose such component for passive RF tags applications fabricated over a flexible plastic substrate, and to this end we also report a proof-of-principle demonstration of its adoption in powering a printed integrated polymer circuit.

In order to realize an organic rectifier on plastic operating at 13.56 MHz, we first focused on its most challenging component, the rectifying diode. We chose inkjet printing as the deposition technique, for both the organic semiconductor and the metal electrodes, as it offers high flexibility in terms of geometrical patterning and a control of the materials deposited volume.

For the device architecture, we selected a Metal-Semiconductor-Metal (MSM) vertical diode (see MSM vertical diode section in Supplementary Information), consisting of a layer of semiconductor sandwiched between two asymmetric, i.e. characterized by a different work function (W_f), metal electrode contacts (Figure 1c).[23] With respect to examples of rectifier based on downscaled FETs biased in transdiode mode,[24] the present diode is much more simple from an architectural and processing point of view, greatly facilitating the integration of rectifiers virtually in any system. The diode is fabricated on a flexible plastic PEN foil. Both electrodes are realized by inkjet printing of a silver nanoparticles based ink, which has a sintering temperature of 120 °C, compatible with the other polymer layers. The semiconductor layer is key to the frequency response. A very common approach to improve the diodes cut-off frequency is by reducing its series resistance (R_S) through the use of thin semiconducting layers and a high charge carrier mobility semiconductor. The latter aspect becomes fundamental when employing printing techniques, as the semiconductor thickness cannot be aggressively scaled because of a typical high level of defectivity, such as pinholes, which can easily lead to high leakages and short circuits. For this reason, the target thickness to allow printing of robust architectures is in the hundreds of nanometers range.**Errore. L'origine riferimento non è stata trovata.** Such

thickness can limit the maximum operating frequency, especially in the case of diodes, where transport occurs at low charge carrier density. In fact, polymer semiconductors are nominally intrinsic and are characterized by a strong carrier density dependence of the mobility.[25] For this reason, the semiconductor choice needs to both allow easy processability and good charge carrier transport properties at low carrier density. To satisfy both requirements, we selected the very well-studied poly{[N,N'-bis(2octyldodecyl)naphthalene-1,4,5,8-bis(dicarboximide)-2,6-diyl]-alt5,5'-(2,2'-bithiophene)}, indicated as P(NDI2OD-T2) in the following.[26] In Figure 1a the chemical structure of P(NDI2OD-T2) is shown. Such semiconductor on the one hand allows to easily formulate inkjet printable inks.[27] On the other, it is very well characterized in field-effect transistors architecture, and can achieve good in-plane (i.e. in the direction parallel to the substrate) electron mobility (> 1 cm^2/Vs) at high carrier density (~ 10^{18}-10^{19} cm^{-3}).[28] Early studies showed that, thanks to a peculiar face-on packing motif, P(NDI2OD-T2) has also good out-of-plane electron transport properties, with electron mobility approaching 10^{-3} cm^2/Vs in a vertical diode configuration, integrating the pristine polymer. [29]

The printed diode process flow is summarized in the following. After printing and sintering a 90 nm thick Ag bottom electrode, a very thin polyethylenimine (PEI) based layer (see Figure 1b for the chemical structure) has been inkjet printed to reduce the Ag work function from 5.04 eV down to 4.54 eV, as measured by Kelvin Probe technique. Such interfacial modification favors electron injection into the lowest-unoccupied molecular orbital (LUMO) of the polymer, lying at around -3.8 eV,[30] and blocking hole injection into the highest-occupied molecular orbital (HOMO).[31] The PEI based-layer plays a key role for the proper rectifying behavior of the diode. On the one hand, it should be thick enough to be effective in reducing the W_f of the electrode. On the other, a too thick PEI based layer leads to a poor injection of electrons from the electrode to the LUMO of the semiconductor, due to its insulating nature.[32] In Figure S5 the merged optical image and confocal profilometry of a PEI printed layer is shown. From the profilometry it is possible to verify that the typical thickness of the PEI layer is in general in

the order of, or less than, tens of nm, with some peaks of 90-100 nm located only at the edges of the printed lines induced by the well-known coffee-ring effect.

As for the printed semiconductor layer, we identified a thickness in the range of few hundreds of nm as a good trade-off between leakage current and series resistance. The diode is completed by printing a 120 nm thick Ag layer on top of the semiconductor, followed by a sintering process at 120 °C. The nominal energetic levels of the system are shown in Figure 1c, while the device structure and top view micrograph of the fully printed diode are shown in Figure 2a-b. The actual cross-section of the device, shown in Figure 2c, was investigated by imaging via SEM a cross-section obtained with a focused ion beam. All the layers are neatly distinguishable, apart from the PEI-based interlayer which is too thin to produce a visible contrast in the image. The current–voltage plot (Figure 2d), which is almost hysteresis free, demonstrates that a high rectification ratio, exceeding 10^6, can be achieved. This is the highest value ever reported for any fully solution-processed diode, including MOs based devices. Such characteristic stems from an efficient injection of charge carriers in the forward bias regime (i.e. bottom Ag/PEI electrode biased negatively with respect to the top Ag electrode) and the good charge transporting properties of the semiconductor, resulting in a forward density current of approximately 330 mA/cm^2 at a bias voltage of 5 V, with a turn-on voltage of $\sim$ 3 V and a series resistance R_S of $\sim$ 5.4 Ωcm^2 (see Figure S1a in the Supporting Information). On the contrary, in the reverse bias, owing to a large barrier for both hole and electron injection, the current density is drastically reduced, to values lower than 300 nA/cm^2. Moreover, such fabrication process allows to achieve very good reproducibility of results, as reported in Figure S1b in which the average I-V curve obtained from measurements of 8 different diodes is shown, along with the standard deviation. For the purpose of this work, all the measurements were carried out in inert atmosphere to simulate an ideal encapsulation. In such conditions diodes are very stable all along extended measurements: in Figure S8 the evolution with time of the On currents (measured at V = 5 V) and Off currents (at V = -5 V) measured every 10 min are plotted

versus time for 300 min. As it can be seen, the On current shows a very mild increase, of only 2 %, and the Off current (the higher noise level is due to the fact that we are measuring nA currents in this case) increases by 15 %.

The dynamic response of the printed diode was tested by integrating it in two kinds of AC-DC rectifying circuits, a *half-wave rectifier* (Figure 3a) and a *double-half-wave rectifier* (Figure 3b). The half-wave rectifier, which is the simplest rectifying circuit, consists of a diode in series with a capacitor. The double-half-wave includes two diodes and two capacitors (see Supporting Information for details and Figure S4 for the optical microscope image of the circuit).[33]

Capacitors were fabricated by sandwiching a bilayer dielectric in between inkjet printed Ag electrodes. The bilayer dielectric stack is composed of a spin coated layer of poly(methyl methacrylate) (PMMA), and a Parylene C layer deposited from vapour. The choice of using a bilayer stack is related to the possibility to reach high capacitance, low leakage currents and high yields, as reported in a recent paper of our group.[34] The areal capacitance of each capacitor is ≅ 4 nF/cm^2 (see Figure S2 in Supporting Information for the complete impedance characterization).

For both rectifiers, the DC output signals (V_{out}) were measured for an AC supply signals at increasing frequencies, from 1 MHz up to 25 MHz, with a constant peak-to-peak amplitude of 10 V. Figure 3c shows the rectified DC output voltages for the half-wave and double-half-wave circuits, measured through an oscilloscope in which the internal resistance (i.e. the input resistance of the instrument) was set to 1 MΩ. For the double-half-wave rectifier, the value of the output is calculated by subtracting V_{out} - (i.e. the rectified voltage of the negative branches of the input AC signal) to V_{out} + (i.e. the rectified voltage of the positive branches of the input). In Figure S3 in Supplementary Information the value of the output voltage in the half-wave rectifier, for different values of the load resistance R_L, is reported. As expected, V_{out} decreases with R_L because the time constant of the RC load decreases, thus leading to a more rapid discharge of the capacitance C. While the V_{out} decreases with increasing frequency, an effect

that can be likely assigned to a reduction of the carrier mobility, both rectifiers do provide a consistent DC output up to 25 MHz, with the double-half-wave rectifier capable of delivering a constant output of 3.8 V at such high frequency.

The result we obtained opens the possibility to adopt our organic rectifiers as electro-magnetic couplers to provide power supply to tags in the HF regime, typical of near-field communication, operating at 13.56 MHz. As an example, the rectified DC output voltage, for the double-half-wave circuits, when the AC input signal is at 13.56 MHz is shown in Figure 3d: V_{out} is almost perfectly constant in time at 4.5 V.

In order to produce a proof-of-concept of the usefulness of such rectifiers in real applications, the operation of a printed integrated polymer circuit was tested when the power supply was provided in AC through the rectifier. We chose to realize for this purpose an integrated D-Flip Flop (DFF), which is a dynamic memory element capable of storing 1 bit, usually employed in sequential digital logic systems.[34] In this work, the DFF was built with 12 transistors (8 p-type and 4 n-type), fabricated over plastic PEN substrate, with the so called "master-slave" configuration (see D-Flip-Flop section in Supplementary Information for further information). Poly(3,4-ethylenedioxithiophene):polystyrene sulphonate (PEDOT:PSS) source, drain and gate contacts, as well as the organic semiconductors, have been patterned by means of inkjet-printing according to a previously reported procedure.[34] The DFF circuit is able to set its output value (V_Q) equal to the input (V_{data}) only in correspondence of the falling edge of the Clock (V_{ck}), which is a periodic waveform used as synchronizing signal in sequential circuits. The correct operation of the integrated circuit powered through the rectifier is shown in Figure 4b, where the value of V_Q is set to V_{data} value and refreshed at every falling edge of the clock signal, as expected.

In conclusion, an organic rectifier based on a fully inkjet printed organic diode and capable of operating in high-frequency regime has been demonstrated. Thanks to the tuning of the barriers at the semiconductor-metal interfaces, the printed diode has a rectification ratio higher than 10^6

with almost negligible hysteresis in DC. When integrated in an organic rectifier, the excellent dynamic properties of the diode allow to rectify sinusoidal AC signals up to 25 MHz, well covering the typical near-field communication range. As demonstrated with a proof-of-concept system in this work, our fully printed polymer diode opens the possibility to couple power to a plastic foil, or, in future, to other non-rigid substrates such as paper, by rectifying a 13.56 MHz AC electromagnetic wave coming from a nearby transmitter, as typically requested in near-field RFID applications. Besides providing a technological solution for fully printed and flexible passive RFIDs, our work offers a plausible path for activating surfaces, powering interactive labels and enabling computation in smart packaging.

Experimental Section

Fully printed vertical organic diodes (total area ~ 22.5 $*10^{-2}$ mm^2), have been fabricated on a 125 μm-thick poly(ethylene 2,6-naphthalate) (PEN) substrate, purchased from Du Pont. Bottom and top electrodes, as well as the injection layer and the organic semiconductor have been all inkjet-printed by means of a Fujifilm Dimatix DMP2831. The layout of the bottom electrode has been designed as the so called *comb structure*: it has 10 interlinked metallic finger of equal length (860 μm) and width (50 μm). The top electrode has a rectangular shape, and its area is 1670 x 900 μm^2 (~ 1.5 mm^2), only partially overlapping but the bottom electrode, as shown in Figure 2b. The overlap between the bottom and the top electrode defines the active area of the vertical diode, which is 0.23 mm^2.

As bottom electrode a layer of a silver nanoparticles-based ink has been printed (Silverjet DGP-40LT-15C, manufactured by Advanced Nano Products – ANP) over the PEN substrate and then syntherized at 120 °C for 1 hour to increase its conductivity.

After that, a polyethylenimine (PEI)-based injection layer has been printed on top of the silver contacts. The ink contains: a) a solution of zinc oxide (ZnO) nanoparticles in IPA (nanoparticles

concentration 2.5% wt); b) ethylene glycol (purchased Sigma Aldrich); c) polyethylenimine (PEI) (branched, purchased from Sigma Aldrich, average $M_w \approx 10\,000$), dissolved in water with a weight concentration of 0.2%. The samples were annealed at 90 °C for 30 minutes in air.

Poly{[N,N'-bis(2octyldodecyl)naphthalene-1,4,5,8-bis(dicarboximide)-2,6-diyl]-alt-5,5'-(2,2'-bithiophene)} (P(NDI2OD-T2) - ActivInk N2200, Polyera) has been used as n-type active material: five layers have been printed from a 1,2-dichlorobenzene (ODCB) based solution, with a concentration of 10 mg/ml. After printing, annealing in nitrogen atmosphere for 1 hour at 110 °C has been performed.

As final step, silver nanoparticles-based ink has been printed as top electrode of the diode structure and then syntherized at 120 °C in nitrogen atmosphere for 1 hour.

In Figure S6, in the Supporting Information, the optical close-up image of the printed diode, and the corresponding topography obtained by confocal profilometry are reported, while in Figure S7 the merged optical image and confocal profilometry of a detail of the semiconductor printed on PEI are shown. The parallel lines of semiconductor printed in partial overlap create ridges that modulate its thickness, from 200 nm to 700 nm, for an average thickness around 400 nm.

Bottom and top electrodes of capacitors (total area ~ 25 mm^2) have been fabricated by means of inkjet printing with silver nanoparticles-based ink (Silverjet DGP-40LT-15C, manufactured by Advanced Nano Products – ANP).

The dielectric stack is composed of a 30 nm spin coated layer of poly(methyl methacrylate) (PMMA) layer (purchased from Sigma Aldrich, average $M_w \approx 120\,000$), and a 450 nm Parylene C layer deposited by means of Chemical Vapour Deposition (CVD) using a Labcoater 2 SCS PDS 2010 (Specialty Coating System).

The organic D-Flip Flop is based on bottom-contact/top-gate organic field effect transistors: Poly(3,4-ethylenedioxithiophene):polystyrene sulphonate (PEDOT:PSS) (Clevios PJ700 formulation, purchased from Heraeus) source and drain contacts have been inkjet-printed by

means of a Fujifilm Dimatix DMP2831. Poly{[N,N'-bis(2octyldodecyl)naphthalene-1,4,5,8-bis(dicarboximide)-2,6-diyl]-alt-5,5'-(2,2'-bithiophene)} (P(NDI2OD-T2) - ActivInk N2200, Polyera) and poly[2,5-bis(7-decylnonadecyl)pyrrolo[3,4-c]pyrrole-1,4(2H,5H)-dione-(E)-1,2-di(2,2′-bithiophen-5-yl)ethene] (29-DPP-TVT) has have been used as n-type and p-type organic semiconductors, both patterned by inkjet-printing. The bilayer gate dielectric stack is composed of a poly(methyl methacrylate) (PMMA) layer, and a Parylene-C layer. PEDOT:PSS gate contacts have been printed on top of the dielectric layer.

The work function of Ag and Ag/PEI electrodes have been measured using a Kelvin Probe microscope (KP020 – KP Technology).

All optical and topography images have been acquired with a Leica DCM 3D Confocal Profilometer, at 50x magnifications. Merged images have been obtained with Adobe Photoshop CS6. Profilometer data have been elaborated with Gwyddion software (plane tilting, profile extraction, file conversion).

The static characterization of the diodes has been performed in an inert nitrogen atmosphere using an Agilent B1500A Semiconductor Parameter Analyzer. For what concerns the capacitors characterization, an Agilent 4294A impedance analyzer has been employed.

Focused ion beam (FIB)-milled cross-sections and scanning electron microscope (SEM) imaging of the organic diode printed on PET were obtained with a Dual Beam FIB/SEM Helios Nano-Lab 600i (FEI). FIB-assisted deposition of Pt (≈ 200 nm nominal thickness) was carried out on the area of interest before FIB-milling of cross-section. SEM images of cross-sections were obtained under a sample tilt angle of 52° (accelerating voltage 10 kV, magnification 250000 X).

The dynamic characterization of the half- and double-half-wave rectifier circuits has been performed using an Agilent 81150A waveform generator to supply the AC input signals with frequencies up to 25 MHz, while for recording the output signals and to provide the load resistance, a Tektronix Digital Phosphor Oscilloscope DPO 2014 oscilloscope has been used.

The dynamic characterization of the DFF powered with the double-half-wave rectifier circuit has been performed using an Agilent 81150A waveform generator to supply the AC input to the rectifier, while the Agilent B1500A Semiconductor Parameter Analyzer has been used for both recording the DFF output signal and to apply the DFF inputs (V_{ck} and V_{data}).

Supporting Information

Supporting Information is available from the Wiley Online Library or from the author.

Acknowledgements

This work was been partially supported by the Italian Ministry for Economic Growth through the project PON Fesr 2017/2020 "Organic Smart Label for IoT", cup B38I170000200008.

F. A. Viola and B. Brigante contributed equally to this work.

Received: ((will be filled in by the editorial staff))
Revised: ((will be filled in by the editorial staff))
Published online: ((will be filled in by the editorial staff))

References

[1] K. Finkenzeller, *RFID Handbook*, Wiley VCH, Munich, Germany **2008**, pp. 21-28.

[2] V. Subramanian, A. de la Fuente Vornbrock, S. Molesa, D. Soltman, H. Y. Tseng, *Organic Electronics II*, Wiley VCH, (Ed. H. Klauk), Stuttgard, Germany **2012**, pp. 237-253.

[3] T. Shimoda, T. Masuda, *Jpn. J. Appl. Phys.* **2014**, *53*, 2S.

[4] a) N. Sani, M. Robertsson, P. Cooper, X. Wang, M. Svensson, P. A. Ersman, P. Norberg, M. Nilsson, D. Nilsson, X. Liu, *Proc. Natl. Acad. Sci. USA* **2014**, *111*, 11943; b) S. Han, X. Dai, P. Loy, J. Lovaasen, J. Huether, J. M. Hoey, A. Wagner, J. Sandstrom, D. Bunzow, O. F. Swenson, I. S. Akhatov, D. L. Schultz, *J. Non-Cryst. Solids* **2008**, *354*, 19-25.

[5] Y. Chu, C. Qian, P. Chahal, C. Cao, *Adv. Sci*. **2018**, *1801653*.

[6] a) X. Yang, P. Chahal, *IEEE 61st Electronic Components and Technology Conf. (ECTC)*, **2011**, pp. 2158-2164; b) C. S. Jones, X. Lu, M. Renn, M. Stroder, W. S. Shin, *Microelectron. Eng.* **2010**, *87*, 3.

[7] a) D. H. Lee, K. Nomura, T. Kamiya, H. Hosono, *IEEE Electron Device Lett.* **2011**, *32*, 12; b) A. Chasin, S. Steudel, K. Myny, M. Nag, T. H. Ke, S. Schols, J. Genoe, G. Gielen, P. Heremans, *Appl. Phys. Lett*. **2012**, *101*, 113505; c) J. Zhang Y. Li, B. Zhang, H. Wang, Q. Xin, A. Song, *Nat. Comm.* **2015**, *6*, 7561; d) I. Choudhary, *Mater. Sci. Eng., B* **2017**, *218*.

[8] Z. Y. Hui, M. Z. Xia, L. H. Li, D. X. Long, *Chin. Phys. B* **2017**, *26*, 4.

[9] a) J. Semple, D. G. Georgiadou, G. Wyatt-Moon, G. Gelink, T. D. Anthopoulos, *Semicond. Sci. Technol.* **2017**, *32*, 12300; b) W. Chem P. Hsu, C. Chie, K. Chang, C. Hsu, C. Chang, W. Lee, W. Chou, H. Hsieh, C. Wu, *J. Phys. D: Appl. Phys.* **2014***, 47,* 365101.

[10] H. Park, H. Kang, Y. Lee, Y. Park, J. Noh, G. Cho, *Nanotechnology* **2012**, *23*, 344006.

[11] K. Abe, K. Suzuki, D. Citterio, *Anal. Chem.* **2008**, *80*, 18.

[12] L. Feng, C. Jiang, H. Ma, X. Guo, A. Nathan, *Org. Electron.* **2016**, *38*.

[13] S. Lai, F. Viola, P. Cosseddu, A. Bonfiglio, *Sensors*, **2018**, *18*, 3.

[14] G. Schwartz, B. C. K. Tee, J. Mei, A. L. Appleton, D. H. Kim, H. Wang, Z. Bao, *Nat. Comm.* **2013**, *4*, 1859.

[15] a) P. Cosseddu, F. Viola, S. Lai, L. Raffo, L. Seminara, L. Pinna, M. Valle, R. Dahiya, A. Bonfiglio, *IEEE Sen. J.* **2014**; b) P. Cosseddu , F. Viola, S. Lai, L. Raffo, A. Bonfiglio, *IEEE Electron Device Lett.* **2014**, *35*, 12.

[16] R. A. Nawrocki, N. Matsuhisa, T. Yokota, T. Someya, *Adv. Electron. Mater.* **2016**, *2*, 4.

[17] L. Zhang, G. Wang, D. Wu, C. Xiong, L. Zheng, Y. Ding, H. Lu, G. Zhang, L. Qiu, *Biosens. Bioelectron*. **2018**, *100*.

[18] a) H. Sirringhaus, T. Kawase, R.H. Friend, T. Shimoda, M. Inbasekaran, W. Wu, E. P. Woo, *Science* **2000**, *29*, 5499; b) U. Zschieschang, H. Klauk, M. Halik, G. Schmid, C. Dehm, *Adv. Mater.* **2003**, *15*, 14.

[19] a) S. Steudel, K. Myny, V. Arkhipov, C. Deibel, S. De Vusser, J. Genoe, P. Heremans, *Nat. Mater.* **2005**, *4*; b) Y. Ai, S. Gowrisanker, H. Jia, I. Trachtenberg, E. Vogel, R. M. Wallace, B. E. Gnade, R. Barnett, H. Stiegler, H. Edwards, *Appl. Phys. Lett.* **2007**, 262105; c) K. Myny, S. Steudel, P. Vicca, J. Genoe, P. Heremans, *Appl. Phys. Lett.* **2008**, *93*, *093305*.

[20] a) D. Im, H. Moon, M. Shin, J. Kim, S. Yoo, *Adv. Mater.* **2011**, *23*, 5; b) C. Kang, J. Wade, S. Yun, J. Lim, H. Cho, J. Roh, H. Lee, S. Nam, D. D. C. Bradley, J. Kim, C. Lee, *Adv. Electron. Mater.* **2016**, *2*, 1500282.

[21] a) S. G. Higgins, T. Agostinelli, S. Markham, R. Whiteman, H. Sirringhaus, *Adv. Mater.* **2017**, *29*, 1703782; b) J. Semple, S. Rossbauer, C. H. Burgess, K. Zhao, L. K. Jagadamma, A. Amassian, M. A. McLachlan, T. D. Anthopoulos, *Small* **2016**, *12*, 15; c) J. Semple, D. G.

Georgiadou, G. Wyatt-Moon, M. Yoon, A. Seitkhan, E. Yengel, S. Rossbauer, F. Bottacchi, M. A. McLachlan, D. D. C. Bradley, T. D. Anthopoulos, *npj Flexible Electron.* **2008**, *2*, 18; d) C. Lin, C. Tsai, H. Lin, L. Chang, Y. Yeh, Z. Pei, Y. Peng, C. Wu, *Org. Electron.* **2011**, *12*.

[22] a) K. E. Lilja, T. G. Backlund, D. Lupo, T. Hassinen, T. Joutsenoja, *Org. Electron.* **2009**, *10*; b) P. S. Heljo, M. Li, K. E. Lilja, H. S. Majumdar, D. Lupo, *IEEE Trans. Electron. Devices* **2013**, *60*, 2; c) P. S. Heljo, K. E. Lilja, H. S. Majumdar, D. Lupo, *Org. Electron.* **2014**, *15*.

[23] a) T. M. Kraft. P. R. Berger, D. Lupo, *Flexible Printed Electron.* **2017**, *2*, 033001; b) R. Hussin. Y. Chen, Y. Luo, *Appl. Phys. Lett.* **2013**, *102*, 093507.

[24] A. Perinot, M. Caironi, *Adv. Sci.* **2019**, *6*, 1801566.

[25] a) C. Tanase, E. J. Meijer, P. W. M. Blom, D. M. de Leeuw, *Phys. Rev. Lett.* **2003**, *91*, 216601; b) Y. Roichman, N. Tessler, *Appl. Phys. Lett.* **2002**, *80*, 1948.

[26] Z. Chen, Y. Zheng, H. Yan, A. Facchetti, *J. Am. Chem. Soc.* **2009**, *131*, 1.

[27] H. Yan, Z. Chen, Y. Zheng, C. Newman, J. R. Quinn, F. Dötz, M. Kastler, A. Facchetti, *Nature* **2009**, *457*.

[28] S. G. Bucella, A. Luzio, E. Gann, L. Thomsen, C. R. McNeill, G. Pace, A. Perinot, Z. Chen, A. Facchetti, M. Caironi, *Nat. Comm.* **2015**, *6*, 8394.

[29] a) G. A. H. Wetzalaer, M. Kuik, Y. Oliver, V. Lemaur, J. Cornil, S. Fabiano, M. A. Loi, P. W. M. Blom, *Phys. Rev. B* **2012**, *86*, 165203; b) R. Steyrleuthner, R. Di Pietro, B. A. Collins, F. Polzer, S. Himmelberger, M. Schubert, Z. Chen, S. Zhang, A. Salleo, H. Ade, A. Facchetti, D. Neher, *J. Am. Chem. Soc.* **2014**, *136*, 11.

[30] L. Gao, Z. Zhang, L. Xue, J. Min, J. Zhang, Z. Wei, Y. Li, *Adv. Mater.* **2015**, *28*, 9.

[31] Y. Zhou, C. Fuentes-Hernandez, J. Shim, J. Meyer, A. J. Giordano, H. Li, P. Winget, T. Papadopoulos, H. Cheun, J. Kim, M. Fenoll, A. Dindar, W. Haske, E. Najafabadi, T. M. Khan, H. Sojoudi, S. Barlow, S. Graham, J. Bredas, S. R. Marder, A. Kahn, B. Kippelen, *Science* **2012**, *336*, 6079.

[32] Y. H. Kim, T. H. Han, H. Cho, S. Y. Min, C. L. Lee, T. W. Lee, *Adv. Funct. Mater.* **2014**, *24*, 24.

[33] B. Razavi, *Fundamentals of Microelectronics*, Wiley VCH, USA **2008**, pp. 89-102.

[34] E. Stucchi, G. Dell'Erba, P. Colpani, Y. H. Kim, M. Caironi, *Adv. Electron. Mater.* **2018**, *4*, 12.

Figure:

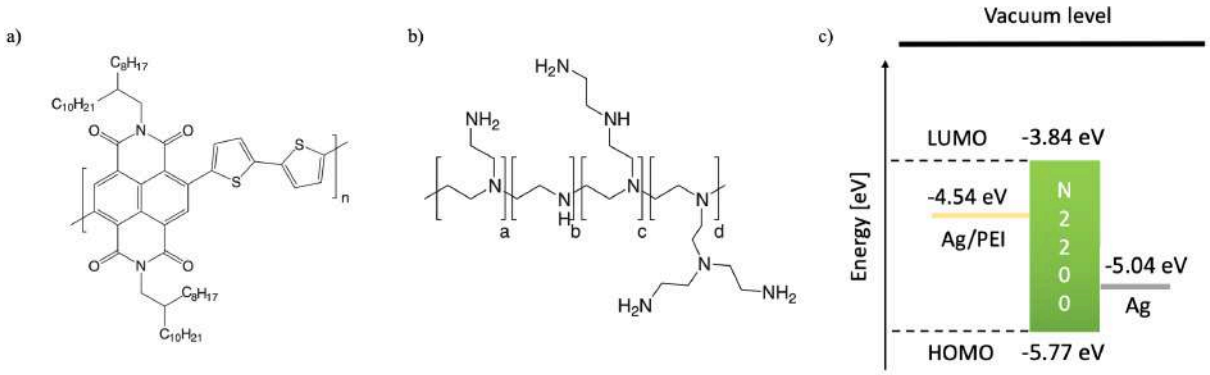

Figure 1. a) Chemical structure of P(NDI2OD-T2) semiconductor. b) Chemical structure of polyethylenimine (PEI). c) Energetic levels of P(NDI2OD-T2) semiconductor HOMO/LUMO and of Ag and Ag/PEI Fermi Level.

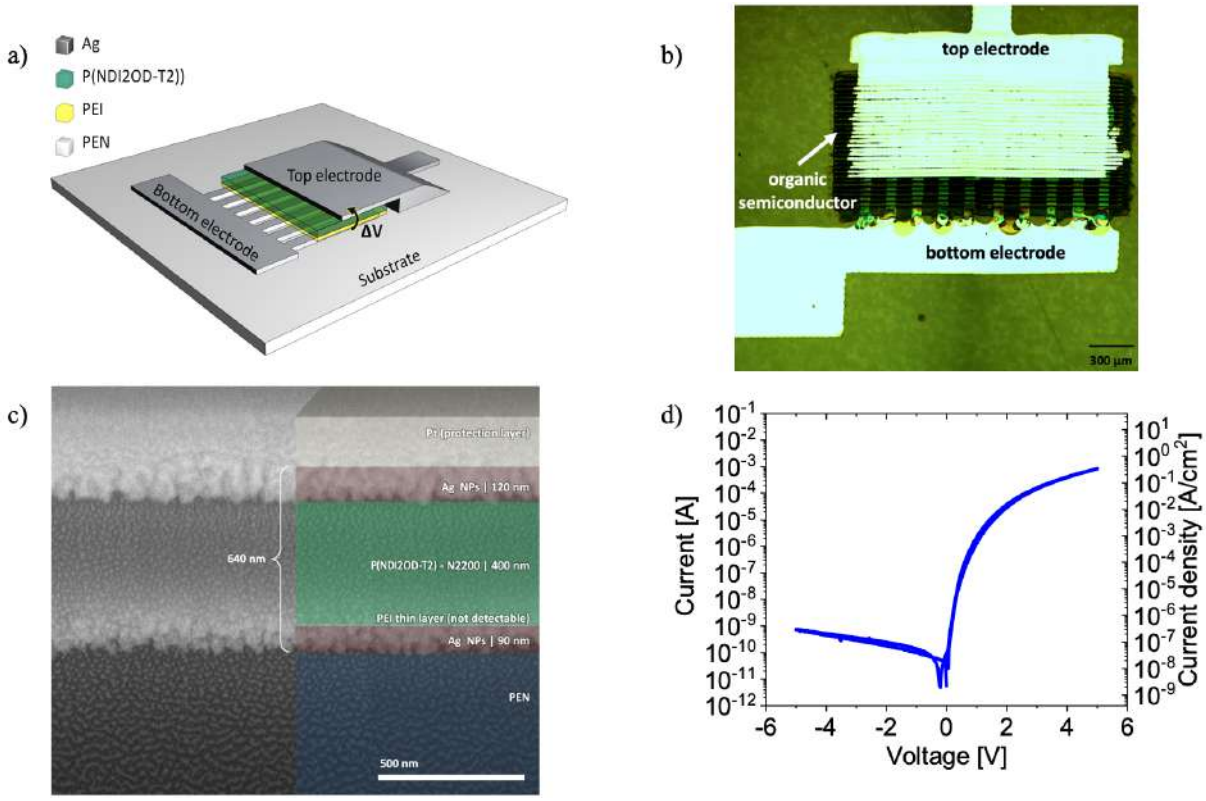

Figure 2. a), b) and c) Device structure, Optical micrograph and FIB cross section of the fully printed organic diode. d) Current-Voltage characteristic curve of a fully printed Ag/PEI/P(NDI2OD-T2)/Ag diode; both forward and backward scans are displayed.

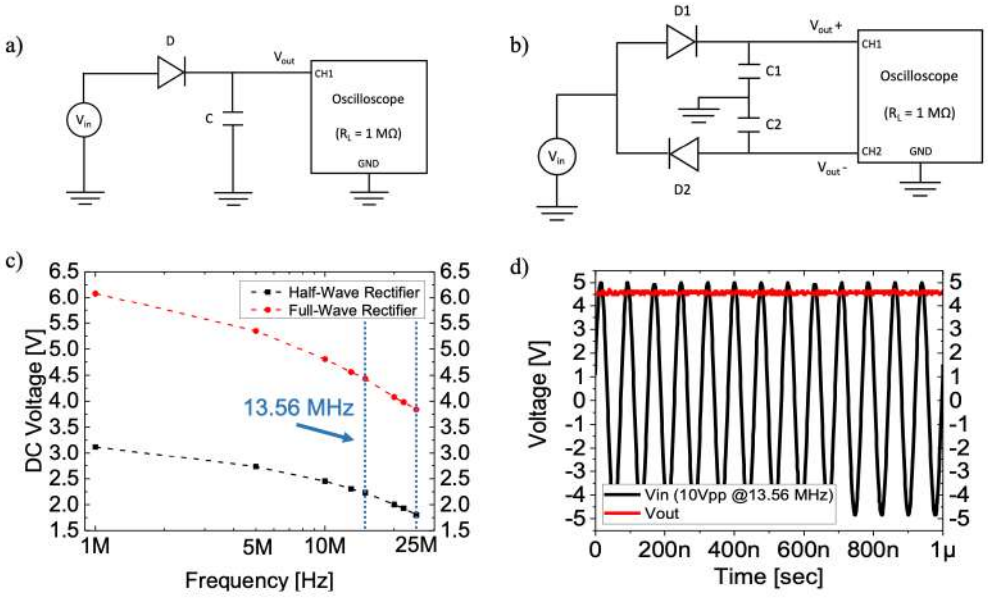

Figure 3. a) Schematic of a half-wave rectifier. b) Schematic of a double-half-wave rectifier. c) Output DC voltage as a function of frequency for a 10 V peat-to-peak sinusoidal input of a half-wave (black symbols) and of a double-half-wave rectifier (red symbols). d) Time response of a double-half-wave rectifier (red line) with a 10 V peat-to-peak sinusoidal input (black line) at 13.56 MHz.

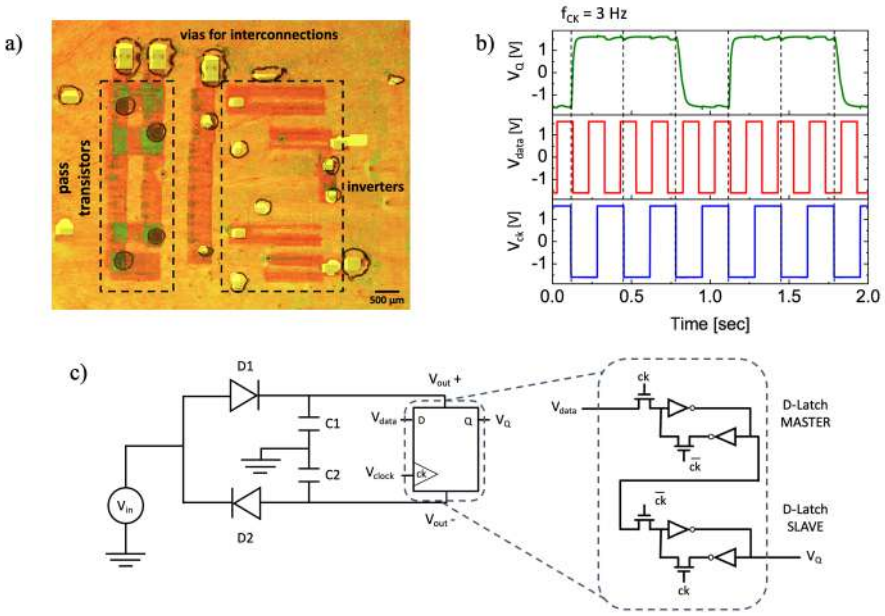

Figure 4. a) Optical micrograph of the integrated DFF circuit printed on PEN. b) Operation of the DFF: output value (V_Q) is set to the input (V_{data}) at each falling edge of the clock. c) Schematic circuit of the DFF employed in this work.

Table of contents: The very first example of a fully inkjet printed organic Schottky diode capable to work at radio frequencies, with a very high rectification ratio, is presented. A rectifier circuit, fabricated by integrating the presented fully printed diodes and capacitors, can successfully rectify a 13.56 MHz sinusoidal AC signal, and supply power to a polymer circuit printed on a plastic foil.

Keywords: printed electronics, RFID, diode, rectifier, organic semiconductors

Fabrizio A. Viola, Biagio Brigante, Paolo Colpani, Giorgio Dell'Erba, Virgilio Mattoli, Dario Natali and Mario Caironi*

Title: A 13.56 MHz Rectifier Based on Fully Inkjet Printed Organic Diodes

ToC figure:

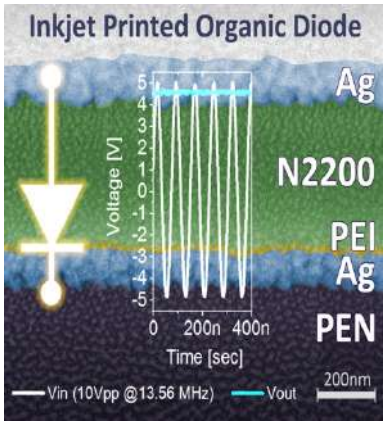

Supporting Information

Title: A 13.56 MHz Rectifier Based on Fully Inkjet Printed Organic Diodes

*Fabrizio A. Viola, Biagio Brigante, Paolo Colpani, Giorgio Dell'Erba, Virgilio Mattoli, Dario Natali and Mario Caironi**

Dr. F. A. Viola, B. Brigante, P. Colpani, Dr. G. Dell'Erba, Prof. Dario Natali, Dr. M. Caironi
Center for Nano Science and Technology @PoliMi, Istituto Italiano di Tecnologia, via Pascoli 70/3, 20133 Milano, Italy.
E-mail: mario.caironi@iit.it
Dr. V. Mattoli
Center for Micro-BioRobotics, Istituto Italiano di Tecnologia, viale Rinaldo Piaggio 34, 50125 Pontedera (PI), Italy
Prof. D. Natali
Dipartimento di Elettronica, Informazione e Bioingegneria, Politecnico di Milano, via Ponzio 34/5, 20133 Milano, Italy

Table S1: Summary and comparison of inorganic and organic diodes, compatible with flexible substrates or fabricated through large-area techniques.

Device	***Active layer material***	***Active layer deposition method***	***Electrodes – Deposition method***	***Frequency***	***on/off current***	***Ref***
Non solution processed						
Schottky diode	a-IGZO	RF sputtering	Al – thermal evaporation Pt – RF sputtering	6300 MHz	10^5	7c
p-n hererojunction diode	IGZO Cu_2O	RF sputtering RF sputtering	ITO – precoated substrate Pt – electron beam evaporation	27 MHz	10^4	9b
Schottky diode	Pentacene	Thermal evaporation	Au – thermal evaporation PEDOT:PSS – spin coating Al – thermal evaporation	50 MHz	10^3	19a
Schottky diode	CuPc	Thermal evaporation	Al – electron beam evaporation Au – electron beam evaporation	14 MHz	$6*10^3$	19b

Schottky diode	Pentacene	Thermal evaporation	Au – electron beam evaporation Al – electron beam evaporation	13.56 MHz	10^3	19c
Schottky diode	C_{60}	Thermal evaporation	Al (+WO_3-HMDS) – thermal evaporation Al (+BCP) – thermal evaporation	700 MHz	10^5	20a
Schottky diode	Pentacene	Thermal evaporation	Au (+PFBT) – thermal evaporation Al – thermal evaporation	1000 MHz	10^7	20b
Partially solution processed						
Schottky diode	SWCNTs	Dielectrophoresis	Ti – electron beam evaporation Au – thermal evaporation	1800 MHz	n.a.	6a
Schottky diode	ZnO	Spin coating	Au – thermal evaporation Al – thermal evaporation	>400 MHz	10^6	21b
Schottky diode	C_{16}IDT-BT	Spin coating	Cr-Au – thermal evaporation Al – thermal evaporation	13.56 MHz	10^6	21a
Schottky diode	C_{60}	Spin coating	Au – thermal evaporation Al – thermal evaporation	400 MHz	10^3	21b
Schottky diode	C_{60}	Spin coating	Au (+MBT/DABT) – thermal evaporation Al – thermal evaporation	13.56 MHz	10^3	21c
Schottky diode	P3HT PQT-12	Spin coating Spin coating	IZO – pre-coated substrate Al – thermal evaporation	14 MHz	$2*10^4$	21d
Partially printed						
Schottky diode	Si microparticles	Screen, inkjet printing	Al – thermal evaporation	1600 MHz	$<10^2$	4a

Schottky diode	PTAA	Gravure printing	Cu – RF sputtering Ag – gravure printing	10 MHz	10^5	22a
Schottky diode	PTAA	Gravure printing	Cu – thermal evaporation Ag – gravure printing	13.56 MHz	n.a.	22b
Schottky diode	PTAA	Gravure printing	Cu – thermal evaporation Ag – gravure printing	13.56 MHz	$<10^3$	22c
Fully printed						
Schottky diode	ZnO	Gravure printing	Ag – gravure printing Al – gravure printing	13.56 MHz	$2.5*10^3$	10
Schottky diode	P(NDI2OD-T2)	Ink-jet printing	Ag (+PEI) – ink-jet printing Ag – ink-jet printing	25 MHz	10^6	This work

Metal-Semiconductor-Metal (MSM) vertical diode.

In a Metal-Semiconductor-Metal (MSM) vertical diode, a layer of semiconductor is sandwiched between two metal electrode contacts characterized by a different work function (W_f).

The asymmetry is required to achieve a proper current rectification: by suitable alignment of the electrodes W_f to the frontier energy levels of the organic semiconductor, it is possible to favor the injection of charge carriers in one biasing direction, and to largely suppress injection in the reverse bias condition.

In reason of that, the materials for the fully printed organic diode have been chosen to finely tune the barriers formed at both metal-semiconductor interfaces, in order to increase as much as possible the rectifying behavior of the system.

The vertical geometry, though more challenging to be achieved through printing techniques, simplifies the scaling of the semiconductor thickness to the sub-micron scale, and therefore reduces the carrier transit time from one electrode to the other with respect to planar diodes, where owing to limitation in printing resolution the inter-electrode spacing is typically in the

micron-scale. In Figure S1, the linear plot of the Current-Voltage static characteristic of the fully printed diode is shown. From this plot, it is possible to extract the value of the series resistance of the diode from the slope of the curve in the forward regime:

$$\frac{\partial I}{\partial V} = \frac{1}{R_S}$$

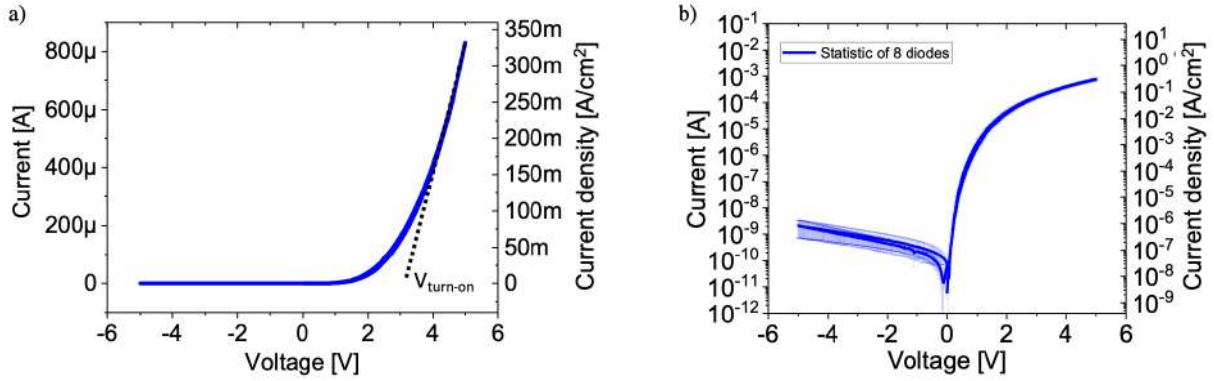

Figure S1. a) Current-Voltage linear plot of a fully printed organic diode. b) Statistic of I-V plot of 8 fully printed organic diodes.

Rectifier circuits.

In order to evaluate the frequency response of the printed diode, two kinds of AC-DC rectifying circuits, the *half-wave rectifier* and a *double-half-wave rectifier*, were tested. The half-wave rectifier consists of a diode in series with a capacitor. It can rectify just one half of each complete sine wave of the AC input in order to convert it into a DC output. During each positive half cycle of the AC sine wave, in which the diode is *forward biased* (i.e. the anode, in this case the top Ag electrode, is positively biased with respect to the cathode, the bottom Ag/PEI electrode), the current flowing through the diode can charge the capacitor. During the each negative half cycle of the input signal the diode is *reverse biased*. Ideally, the capacitor is isolated and stores the accumulated charge, therefore maintaining a fixed voltage. In reality, it can discharge through the parasitic paths towards ground. The full-wave rectifier includes two diodes and two capacitors and allows to rectify both the positive and the negative peak of the AC input signal, thus nominally achieving double of the DC output of the half-way rectifier.

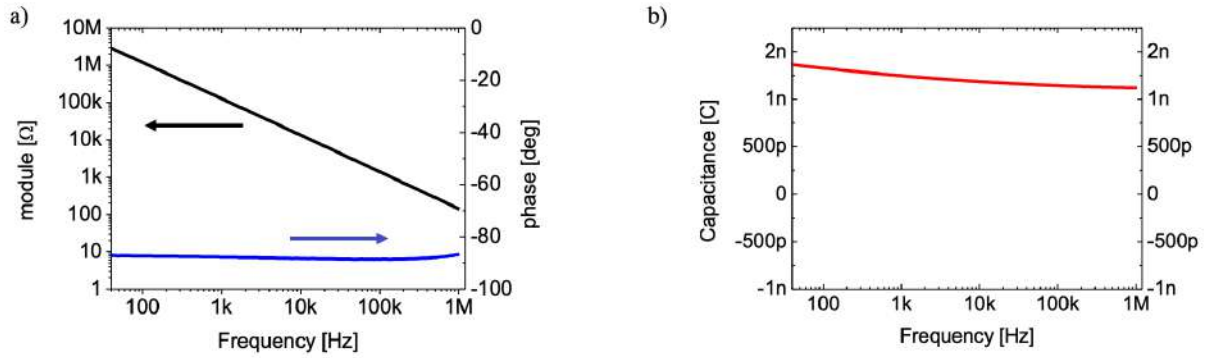

Figure S2. a) Bode plot with module and phase of a Parylene C/PMMA capacitor. b) Capacitance values as a function of frequency.

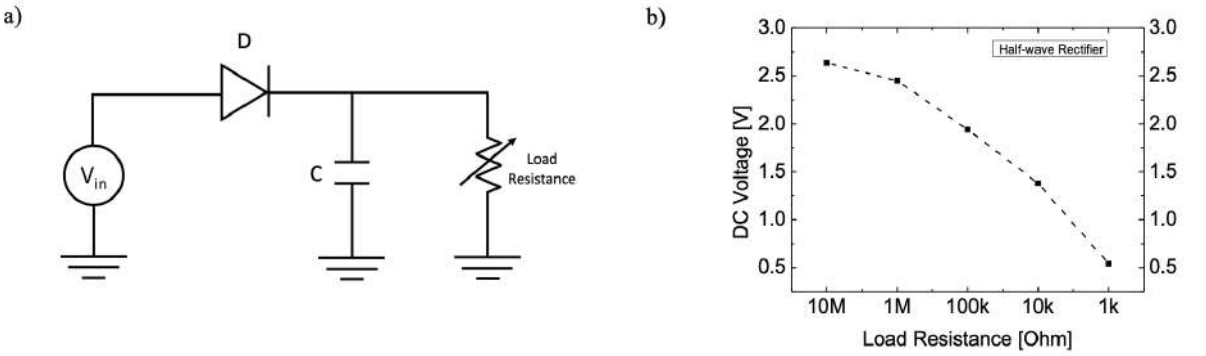

Figure S3. a) Schematic of the half-wave rectifier connected with a variable resistor. b) DC voltage as a function of the load resistance for a sinusoidal AC input signal of 10 V peak-to-peak at 13.56 MHz.

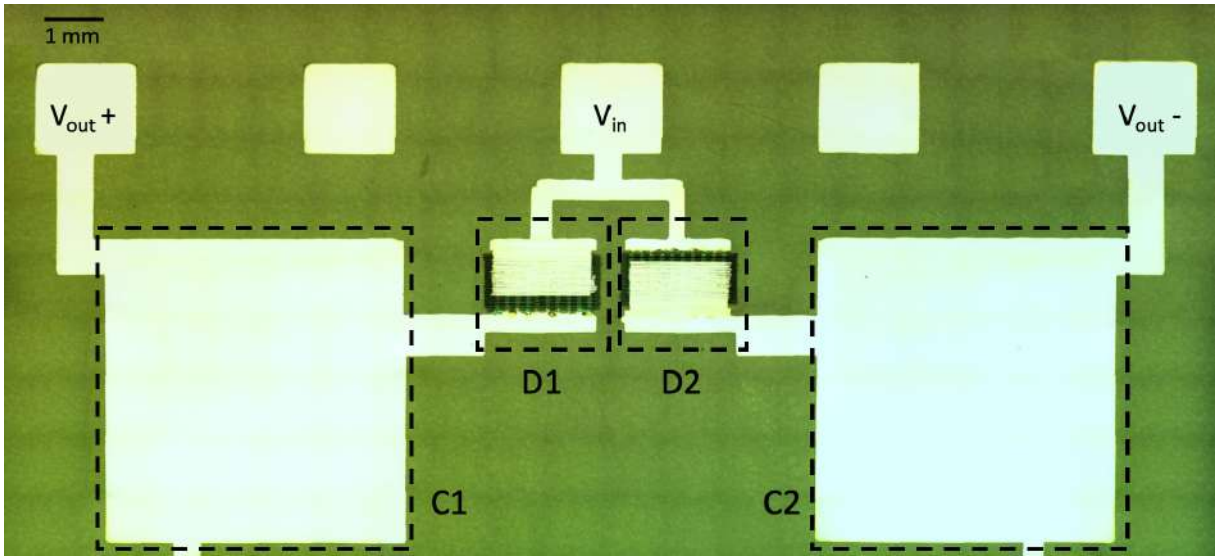

Figure S4. Optical micrograph of the double half-wave rectifier circuit on PEN substrate: C1 and C2 are the capacitors while D1 and D2 are the two diodes.

D-Flip-Flop

The D-Flip-Flop (DFF) is one of the basic electronic circuits used to store information. In this work, we chose a Master-Slave DFF which is implemented by making use of two D-Latch circuits. The D-Latch circuit is composed of two inverters and two transmission gates, working with opposite phases. The operation of the D-Latch can be divided into two phases, the *hold* phase and the *transparent* phase.

- *Hold phase*: the clock signal is low, the device holds stably as output the signal received as input on the falling edge of the clock.
- *Transparent phase*: the clock signal is high and the input signal passes through the circuit and reaches the output.

The peculiarity of the D-Latch is that the output signal is sensitive to any change of the input signal during the transparent phase while, during the hold phase, it is completely insensitive to input changes. The DFF was built with 12 transistors (8 p-type and 4 n-type) with two D-Latches connected in series and with opposite clock signals ("master-slave" configuration), so that when one is in its transparent phase, the other is in hold phase, and vice versa.

The circuit is able to set its output value to the input, only in correspondence of the falling edge of the clock.

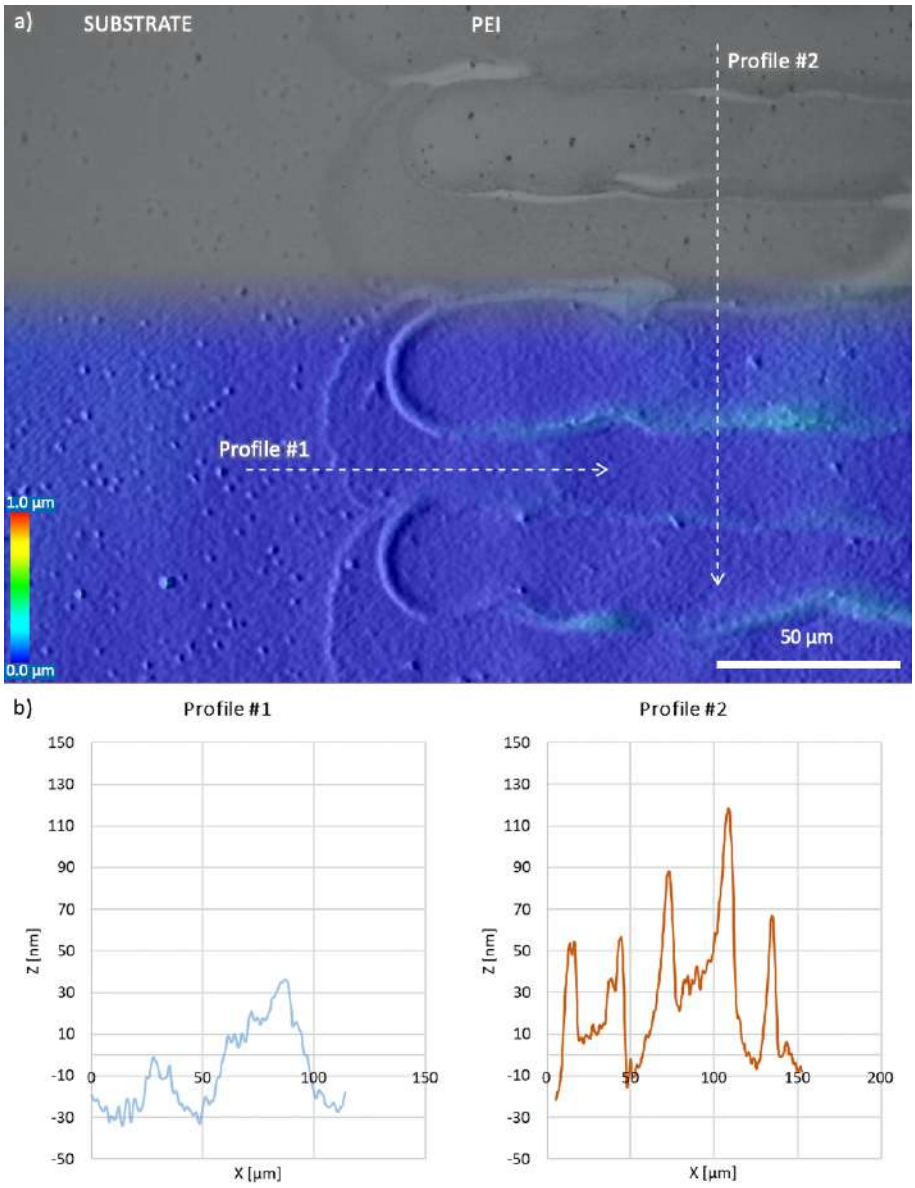

Figure S5. a) Merged optical image and confocal profilometry of a detail of PEI printed on PEN substrate (including transition zone). b) Plots of two indicative surface profiles shown in a), as indicated by dashed arrows. From the profilometry it is possible to verify that the typical thickness of the PEI layer is in general in the order of, or less than, tens of nm. Nevertheless, the printing process induces coffee-ring effect that modulates the thickness of the PEI, reaching up to about 100 nm for specific areas along the deposition direction.

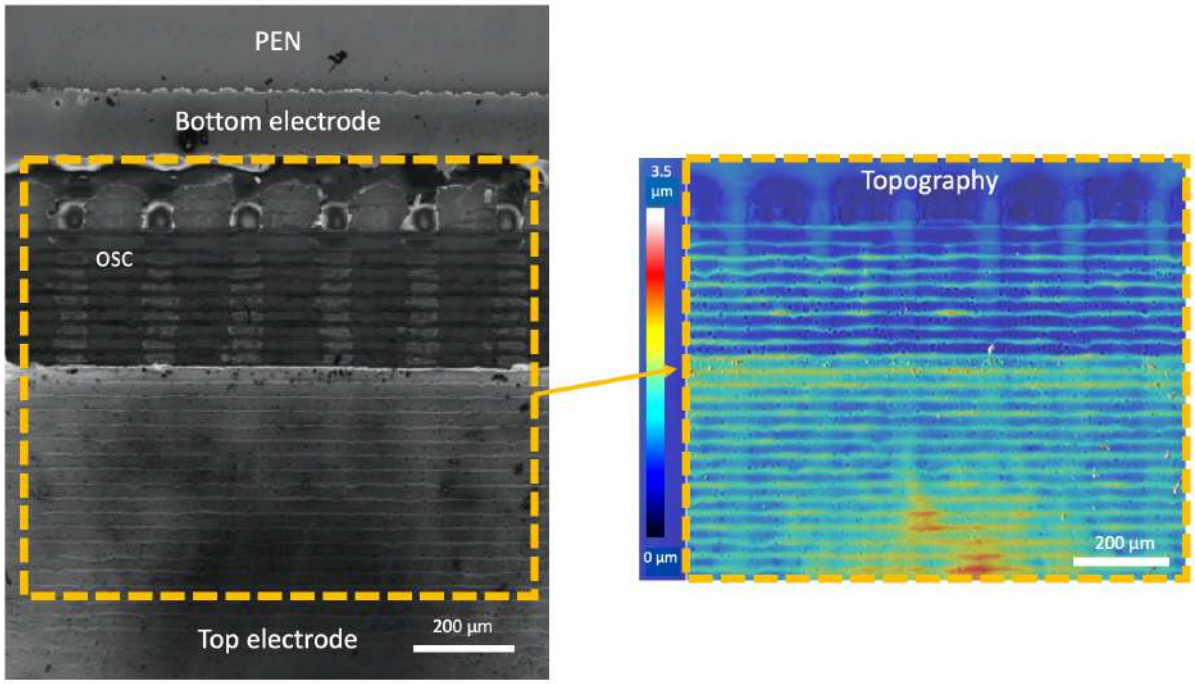

Figure S6. Optical close-up image of printed diode device, and related topography obtained by confocal profilometry (see inset).

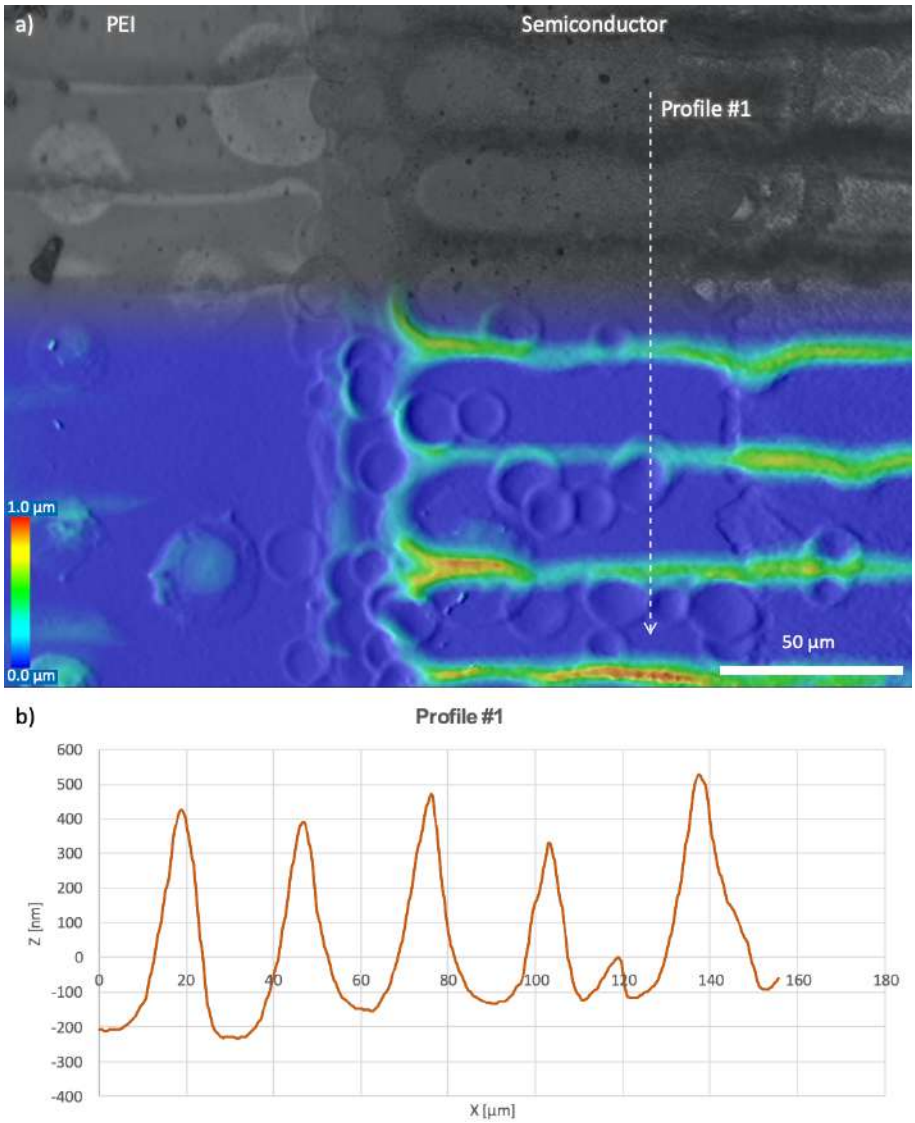

Figure S7. a) Merged optical image and confocal profilometry of a detail of semiconductor printed on PEI, including transition zone. b) Plots of the indicative profile of surface shown in a), as indicated by dashed arrows.

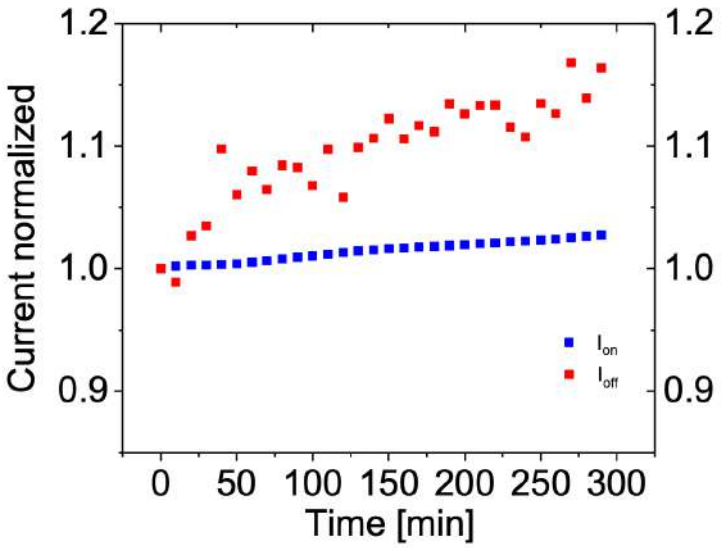

Figure S8. Stability of the fully printed diode in inert atmosphere. Normalized values of On and Off currents (measured at V = 5V and V = -5V respectively) plotted versus time for 300 min.